Microchimica Acta (2022) 189: 129
https://doi.org/10.1007/s00604-022-05246-0

ORIGINAL PAPER

MicroRNA-21 electrochemiluminescence biosensor based on Co -MOF–*N*-(4-aminobutyl)-*N*-ethylisoluminol/$Ti_3C_2T_x$ composite and duplex-specific nuclease-assisted signal amplification

Yang Jiang[1] · Rong Li[2] · Wenyu He[1] · Qian Li[1] · Xia Yang[1] · Sijia Li[1] · Wanqiao Bai[2] · Yan Li[1]

Received: 18 October 2021 / Accepted: 22 February 2022 / Published online: 3 March 2022

Abstract

A novel electrochemiluminescence (ECL) biosensor for the determination of microRNA-21 (miRNA-21) was developed, based on a hybrid luminescent Co-MOF-ABEI/$Ti_3C_2T_x$ composite as an ECL luminophore combined with a duplex-specific nuclease (DSN)-assisted signal amplification strategy. The synthesized Co-MOF-ABEI/$Ti_3C_2T_x$ composite carrying *N*-(4-aminobutyl)-*N*-ethylisoluminol (ABEI) exhibited strong and stable ECL in the presence of reactive oxygen species (ROS). The ECL biosensor was fabricated by adsorbing Co-MOF-ABEI/$Ti_3C_2T_x$ onto a glassy carbon electrode and covalently coupling the probe DNA onto the surface of the Co-MOF-ABEI/$Ti_3C_2T_x$-modified electrode. In the presence of the target miRNA-21, the DSN selectively cleaved the complementary DNA section (S1) to miRNA-21, resulting in the release of the transduction section (S2) and the reuse of miRNA-21 in the subsequent amplification cycle. The interaction of the stem-loop structure of the probe DNA with the Co-MOF-ABEI/$Ti_3C_2T_x$-modified glassy carbon electrode with S2 strands led to the opening of the annular part of the probe DNA. Then, the opened guanine (G)-rich sequences of probe DNA were exposed and folded into a hemin/G-quadruplex DNAzyme in the presence of hemin. The catalysis of H_2O_2 to ROS by the hemin/G-quadruplex DNAzyme significantly enhanced ECL intensity, and this intensity was logarithmically proportional to the concentration of target miRNA-21 between 0.00001 and 10 nM, having a limit of detection of 3.7 fM. The designed ECL biosensor can detect miRNA-21 extracted from HeLa cells, indicating its promising application in clinical diagnosis and disease prognosis analysis.

Keywords MicroRNA-21 · Electrochemiluminescence · Modified glassy carbon electrode · Metal–organic frameworks · Duplex-specific nuclease

Introduction

MicroRNAs (miRNAs) are a series of endogenous, small, noncoding, single-stranded RNAs having lengths of 18–25 nucleotides [1]. miRNAs play important regulatory roles in various biological processes and are biomarkers for early disease diagnosis [2]. Many studies have demonstrated that the abnormal expression of miRNAs is associated with a wide variety of diseases, such as cancer [3], diabetes [4], muscle disorders [5], and neurological disorders [6]. Therefore, this emerging biomarker has been extensively studied. However, because of the low concentration of miRNA in biological samples, the development of techniques for the sensitive and specific detection of miRNA is crucial [7]. To date, various methods have been developed for the detection of miRNAs, including electrochemical [8], chemiluminescence [9], fluorescence [10], colorimetry [11], and electrochemiluminescence (ECL) [12, 13]. Among these methods,

Yang Jiang, Rong Li and Wenyu He These authors contributed equally to this work.

✉ Wanqiao Bai
baiwanqiao@163.com

✉ Yan Li
yanli@nwu.edu.cn

[1] Key Laboratory of Synthetic and Natural Functional Molecule Chemistry of the Ministry of Education, College of Chemistry and Materials Science, Northwest University, Xi'an 710127, People's Republic of China

[2] Department of Chemistry and Chemical Engineering, Laboratory of New Energy & New Function Materials, Key Laboratory of Analytical Technology and Detection, Yan'an University, Shaanxi 716000, People's Republic of China

ECL has many advantages, such as high detection sensitivity, low cost, easy operation, and rapid response times, and it has become the latest generation of biomedical diagnostic and detection methods [14].

To date, many nucleic acid signal amplification strategies have been applied to develop sensitive ECL biosensors for miRNA detection, including the polymerase chain reaction (PCR) [15], rolling circle amplification [16], target-catalyzed hairpin assembly [17], duplex-specific nuclease (DSN)-assisted amplification [18, 19], and other amplification strategies [20, 21]. Among these strategies, DSN-assisted amplification has attracted considerable research attention owing to its strong ability for recycling amplification. DSN is capable of cleaving DNA into DNA fragments in DNA-RNA heteroduplexes while preventing the cleavage of the RNA strand, resulting in the release of target RNA to regenerate a new heteroduplex structure for cyclic cleavage. Therefore, the DSN-assisted target recycling signal amplification strategy can be applied for the ultrasensitive detection of miRNA. However, it is usually difficult to separate released nucleic acid strands after DSN cleavage. As a solution, magnetic bead (MB) technology has emerged. MBs can rapidly separate targets from interfering substances [22] and can be modified with different functional groups to capture different target molecules [23].

Luminol is a classic organic ECL luminophore that can be applied in aqueous media and has become the most popular ECL luminophore because of its markedly low oxidation potential, low cost, nontoxicity, and high light-emitting quantum yield [24]. In the present study, *N*-(aminobutyl)-*N*-ethylisoluminol (ABEI) was selected as the ECL signal probe because of its additional active primary amino groups, which enable immobilization by reaction with other reagents [25]. To enhance the ECL performance of the ABEI-H_2O_2 ECL system, strategies based on catalyzing H_2O_2 to generate reactive oxygen species (ROS), such as $O^{\cdot-}$ and ·OH radicals, have been used [26]. The hemin/G-quadruplex, a catalytic nucleic acid structure formed by inserting hemin into a guanine-rich single-stranded nucleic acid, exhibits distinctive enzyme-mimic activity to catalyze the conversion of H_2O_2 to ROS [27]. Therefore, the features of the hemin/G-quadruplex can be employed to improve the ECL performance of the ABEI-H_2O_2 system.

To date, the use of ABEI has encountered several drawbacks such as limited immobilization and complex preparation. Metal–organic frameworks (MOFs) are porous crystalline materials having a high specific surface area, permanent porosity, adjustable functionality, and thermal stability and have been widely used in various fields [28]. In particular, MOFs have shown considerable potential in ECL applications because luminophores can be effectively immobilized on MOFs [29]. For example, Ge et al. developed an effective method to enhance the ECL efficiency of the luminol system by combining ZIF-67 MOF with luminol-covered Ag nanoparticles [30]. Recently, our group successfully synthesized a $Ru(bpy)_3^{2+}$-functionalized MOF (Ru@MOF; bpy: 2,2′-bipyridine) to fabricate ECL platforms for m^6A RNA determination [31]. However, the poor intrinsic electrical conductivity of MOFs markedly hinders their application as electrode materials. Therefore, it is necessary to construct new luminescent MOFs with improved electrical conductivities for biological analysis.

In the present study, a sensitive ECL biosensing platform for the determination of miRNA-21 was fabricated using a Co-MOF-ABEI/$Ti_3C_2T_x$ composite as an ECL luminescent substrate combined with a DSN-assisted target recycling signal amplification strategy. $Ti_3C_2T_x$ is a highly suitable matrix for the fabrication of advanced biosensing platforms owing to its unique morphology, excellent biocompatibility, and conductivity [32]. The ABEI luminophore conjugated with 2-aminoterephthalic acid (NH_2-BDC-ABEI) acts as an organic ligand to form Co-MOF-ABEI, which carries abundant luminophores owing to the large surface area of the Co-MOFs. Furthermore, studies have reported Co-MOFs having marked catalytic ability for biosensing applications [33]. First, NH_2-BDC-ABEI as the organic ligand, $Co(NO_3)_2{\cdot}6H_2O$ as the metal ion source, and highly conductive $Ti_3C_2T_x$ were mixed together to synthesize a Co-MOF-ABEI/$Ti_3C_2T_x$ composite in a one-pot process. Meanwhile, in the DSN-assisted target recycling signal amplification strategy, a single miRNA-21 strand triggered the generation of multiple transduction sections (S2) that can markedly improve the sensitivity. Subsequently, the released S2 strands hybridized with numerous G-rich hairpin DNA strands (probe DNA) captured on the Co-MOF-ABEI/$Ti_3C_2T_x$-modified GCE (Co-MOF-ABEI/$Ti_3C_2T_x$/GCE), thus opening the annular part of the probe DNA. Then, in the presence of hemin, hemin/G-quadruplex complexes were generated, and these catalyzed the conversion of H_2O_2 to ROS to amplify ECL emission. Benefiting from the strong ECL emission of Co-MOF-ABEI/$Ti_3C_2T_x$ and DSN-assisted target recycling amplification, the designed ECL biosensor showed high sensitivity and selectivity for miRNA-21 detection.

Experimental

All reagents and apparatus are presented in the supporting information.

Synthesis of $Ti_3C_2T_x$

$Ti_3C_2T_x$ was prepared by selectively etching Al layers from Ti_3AlC_2 powder following a previously described method [34]. Briefly, 2 g of Ti_3AlC_2 powder was gradually added to a plastic beaker containing 40 wt% concentrated HF acid (30 mL) and stirred at 45 °C for 24 h. The prepared mixture was separated by centrifugation and rinsed repeatedly with distilled water and ethanol until the pH of the mixture

reached 5.0–6.0. Finally, the obtained black precipitate of $Ti_3C_2T_x$ was dried at 60 °C for 12 h.

Preparation of the Co-MOF-ABEI/$Ti_3C_2T_x$ composite

The Co-MOF-ABEI/$Ti_3C_2T_x$ composite was synthesized according to a previously described method with a few modifications [35]. Initially, 0.1417 g of ABEI and 0.1449 g of 2-aminoterephthalic acid (NH_2-BDC) were mixed with 15 mL of *N*,*N*-dimethylformamide (DMF). Next, 1.0 mL of 1% glutaraldehyde (GA) was added dropwise into the mixture, which was magnetically stirred for 2 days in the dark to crosslink NH_2-BDC and ABEI and form the NH_2-BDC-ABEI ligand. Next, 0.12 g of the prepared $Ti_3C_2T_x$ was added to 20 mL of DMF and sonicated for 30 min to obtain a homogeneous black dispersion.

To prepare the Co-MOF-ABEI/$Ti_3C_2T_x$ composite, the NH_2-BDC-ABEI and $Ti_3C_2T_x$ mixtures were stirred together for 10 min. Next, 0.2330 g of $Co(NO_3)_2{\cdot}6H_2O$ was added to the above mixture, and it was heated at 140 °C for 4 h. Then, the obtained Co-MOF-ABEI/$Ti_3C_2T_x$ was collected by centrifugation, washed with DMF and ethanol three times, and then dried. Finally, the obtained Co-MOF-ABEI/$Ti_3C_2T_x$ was dispersed in 1.0 mL of ultrapure water and stored at 4 °C.

Fabrication of MB-S1:S2 bioconjugates

A 50-μL suspension containing 10 mg/mL carboxyl MBs was washed with 50 mM 2-(*N*-morpholino)ethanesulfonic acid (MES) buffer (pH 6.0, 0.01% Triton X-100) three times. Next, a solution containing 1-ethyl-3-(3-dimethylaminopropyl)carbodiimide (50 mg/mL) and *N*-hydroxysulfosuccinimide (50 mg/mL) was mixed with the MB suspension and incubated at about 25 °C for 15 min to activate the carboxylate groups. Next, 200 μL of 2 μM S1:S2 strand was added to the above mixture and stirred for 3 h to form MB-S1:S2 bioconjugates. After magnetic separation, the MB-S1:S2 bioconjugates were washed three times with 50 mM MES buffer. The obtained MB-S1:S2 bioconjugates were resuspended in 100 μL phosphate-buffered saline (PBS1, 0.1 M, pH 7.0) and stored at 4 °C until further use. The synthesized MB-S1:S2 bioconjugates were characterized by UV–vis spectroscopy (UV–vis absorption spectra of S1:S2 strand and MB-S1:S2 bioconjugates are shown in Fig. S1), which indicated that the MB surface had been successfully modified with S1:S2 strands.

Generation of S2 strands

The total volume of the reaction system was 100 μL, including 10 μL of MB-S1:S2 bioconjugates, 10 μL of 10 × DSN buffer (500 mM Tris–HCl, pH 8.0, 50 mM $MgCl_2$, and 10 mM dithiothreitol), 1 μL of 0.1 U DSN in 50 mM Tris–HCl buffer (pH 8.0) and 50% glycerol, and 69 μL of diethylpyrocarbonate-treated water. Next, 10 μL of different concentrations of miRNA-21 was added, and the reaction system was incubated at 50 °C for 70 min with gentle mixing. Finally, a DSN stop solution containing 5 mM ethylenediaminetetraacetic acid was introduced to stop the cyclic DSN reaction, and the solution containing S2 strands was dissociated and collected from MBs with a magnet for the ECL measurement experiments.

Fabrication of the biosensing electrode

A glassy carbon electrode (GCE, 3.0 mm diameter) was polished with 0.3 and 0.05 μm aluminum oxide (Al_2O_3) powder to achieve a clean and smooth surface. Next, 10 μL of the Co-MOF-ABEI/$Ti_3C_2T_x$ dispersion was spin-coated onto the surface of the cleaned GCE with a microsyringe and allowed to dry at room temperature to obtain the Co-MOF-ABEI/$Ti_3C_2T_x$/GCE. Subsequently, a drop (3 μL) of chitosan (CS) solution (0.5%) was placed on the surface of Co-MOF-ABEI/$Ti_3C_2T_x$/GCE to obtain CS/Co-MOF-ABEI/$Ti_3C_2T_x$/GCE. For the immobilization of the probe DNA, CS/Co-MOF-ABEI/$Ti_3C_2T_x$/GCE was immersed in GA solution (5%) for 2 h and then carefully rinsed with PBS2 buffer (0.01 M, pH 7.4) to form GA/CS/Co-MOF-ABEI/$Ti_3C_2T_x$/GCE. Subsequently, a drop (10 μL) of probe DNA (1 μM) was placed on the surface of GA/CS/Co-MOF-ABEI/$Ti_3C_2T_x$/GCE and incubated at 4 °C for 12 h to obtain probe DNA/GA/CS/Co-MOF-ABEI/$Ti_3C_2T_x$/GCE. The -NH_2 group at the 5′ end of the probe DNA reacted with the -CHO group of GA on the modified electrode by forming Schiff bases [36]; thus, the probe DNA was covalently immobilized onto the GA/CS/Co-MOF-ABEI/$Ti_3C_2T_x$-modified electrode. Next, the obtained probe DNA/GA/CS/Co-MOF-ABEI/$Ti_3C_2T_x$/GCE was immersed in 1 mM monoethanolamine (MEA) solution for 2 h at 4 °C to neutralize the unreacted aldehyde groups, followed by rinsing to remove the unreacted MEA. The resulting probe DNA/GA/CS/Co-MOF-ABEI/$Ti_3C_2T_x$/GCE was then thoroughly washed with PBS2 (pH 7.4) and used as the ECL biosensing electrode for miRNA-21.

ECL measurements

Because the concentration of S2 strands is directly proportional to the concentration of target miRNA-21, the amount of target miRNA-21 can be determined by measuring the number of S2 strands. The biosensing electrode was immersed in the obtained solution containing S2 strands and incubated for 1 h to obtain the S2/probe DNA/GA/CS/Co-MOF-ABEI/$Ti_3C_2T_x$/GCE, followed by washing to remove the unhybridized S2 strands. Finally, 10 μL

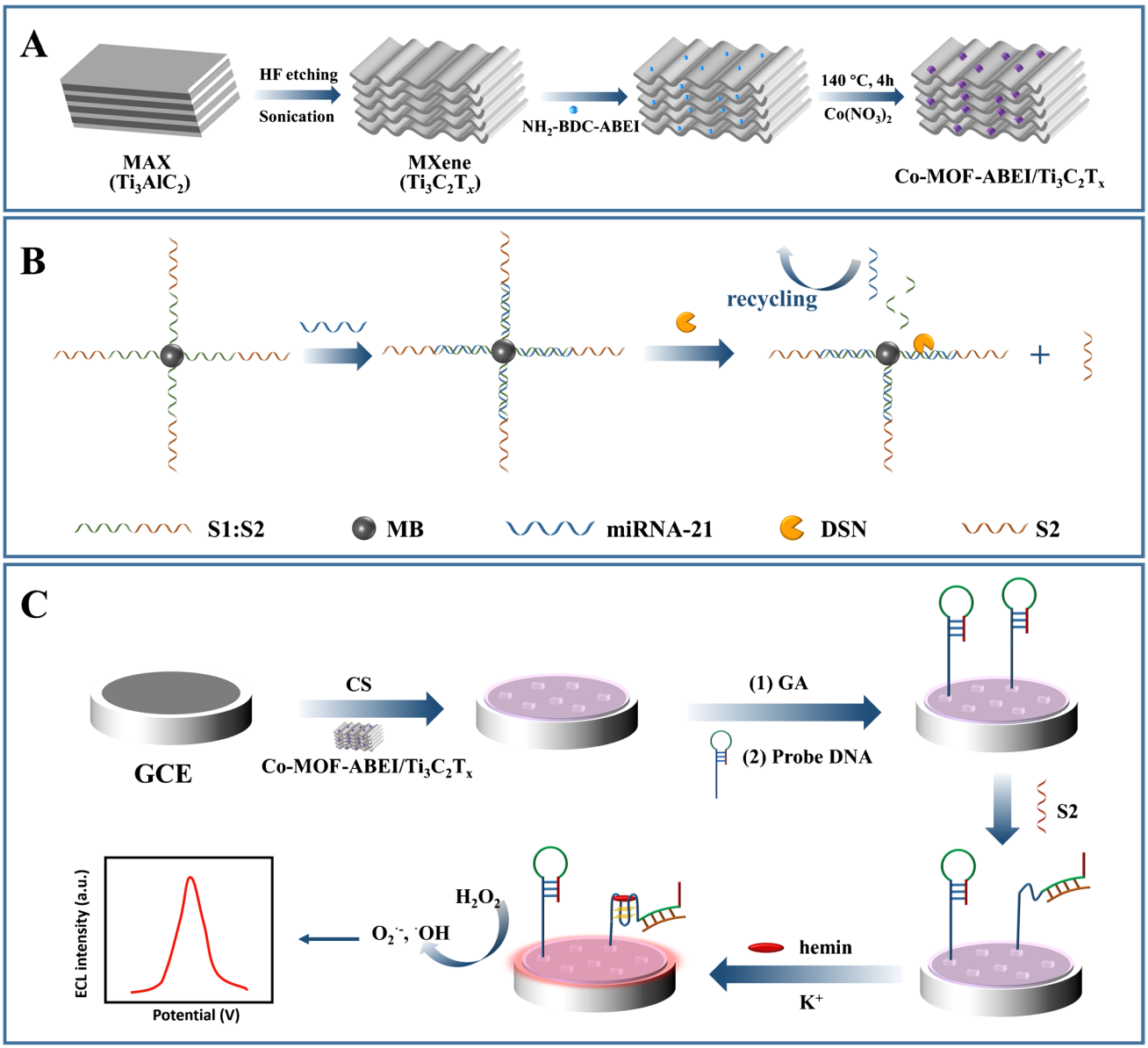

Scheme 1 Schematic of the fabricated ECL biosensing platform for miRNA-21 detection. **A** Preparation of the Co-MOF-ABEI/$Ti_3C_2T_x$ composite. **B** DSN-assisted target recycling amplification strategy for S2 strand release. **C** Construction of the ECL biosensor based on Co-MOF-ABEI/$Ti_3C_2T_x$ and hemin/G-quadruplex complexes

of hemin (0.5 mM) containing potassium ions was used to incubate the S2/probe DNA/GA/CS/Co-MOF-ABEI/$Ti_3C_2T_x$/GCE at 4 °C for 1 h to form the hemin/G-quadruplex structure. The obtained hemin /S2/probe DNA/GA/CS/Co-MOF-ABEI/$Ti_3C_2T_x$/GCE was immersed in 1.0 mL of PBS1 (pH 7.0) containing 2 mM of H_2O_2 for ECL measurements, and the potential was scanned from 0 to + 0.6 V at a scan rate of 0.1 $V{\cdot}s^{-1}$; the photomultiplier tube voltage was set at − 800 V. The maximum ECL intensity at a potential of approximately + 0.52 V was recorded.

Results and discussion

Principle of the ECL biosensor

Details of the fabrication of the biosensor for miRNA-21 detection are shown in Scheme 1. Scheme 1A shows the synthetic route of Co-MOF-ABEI/$Ti_3C_2T_x$ composite as ECL emitter. Scheme 1B illustrates the DSN-assisted target recycling amplification strategy. The S1:S2 strands, which have two main sections, the recognition section (S1)

and the transduction section (S2), were modified onto carboxyl MBs. The S1 section strand matched the target miRNA-21 to form DNA-RNA heteroduplexes at the 5′ end, whereas the remaining transduction S2 strand was at the 3′ end. The DSN enzyme can cleave the DNA in DNA-RNA heteroduplexes with high specificity. Thus, when miRNA-21 was introduced to the DSN cycle amplification process, it hybridized with S1 in the S1:S2 strand. After adding the DSN enzyme, S1 in the DNA-RNA heteroduplexes was cleaved, and miRNA-21 was released sequentially. The released miRNA-21 constantly triggers the next amplification cycle while releasing the more S2 strands. Scheme 1C illustrates the entire detection process. First, a low ECL signal was observed for the Co-MOF-ABEI/$Ti_3C_2T_x$-modified GCE probably because of the limited production of ROS. After DSN cyclic amplification and magnetic separation, the released S2 strands hybridized with the hairpin probe DNA on the biosensing electrode, which resulted in the opening of the annular structure of probe DNA. Because the hairpin probe DNA contains a G-rich sequence, the exposed G-rich sequences can further form a G-quadruplex in the presence of hemin. Finally, the hemin/G-quadruplex can catalyze the conversion of H_2O_2 to ROS; consequently, ECL intensity is significantly enhanced. Thus, miRNA-21 can be quantified based on the increase in ECL signal intensity.

Characterization

The morphological characteristics of the prepared materials were characterized using scanning electron microscopy (SEM). As shown in Fig. 1A, the laminated $Ti_3C_2T_x$ that was etched and exfoliated from the MAX Ti_3AlC_2 phase exhibits a typical accordion-like layer structure. Figure 1B clearly shows that the Co-MOF-ABEI grew on $Ti_3C_2T_x$ sheets in situ. Next, X-ray photoelectron spectroscopy (XPS) was used to identify the chemical composition of the Co-MOF-ABEI/$Ti_3C_2T_x$ composite. As shown in Fig. 1C, the resulting spectra showed the presence of C, N, O, Co, and Ti. Additionally, the elemental mapping results were consistent with XPS findings (Fig. S2), which also confirmed the presence of C, N, O, Co, and Ti in Co-MOF-ABEI/$Ti_3C_2T_x$, and all the elements were homogeneously distributed throughout the composite. The successful synthesis of the Co-MOF-ABEI/$Ti_3C_2T_x$ composite was further confirmed by UV–vis absorption spectra. As illustrated in Fig. 1D, ABEI yields two absorption peaks at 230 and 267 nm, respectively. However, redshifts in the absorption peaks of Co-MOF-ABEI/$Ti_3C_2T_x$ were observed because of the cross-linking between ABEI and NH_2-BDC, which increased the degree of conjugation. The characterization results indicate that the Co-MOF-ABEI/$Ti_3C_2T_x$ composite had been successfully prepared.

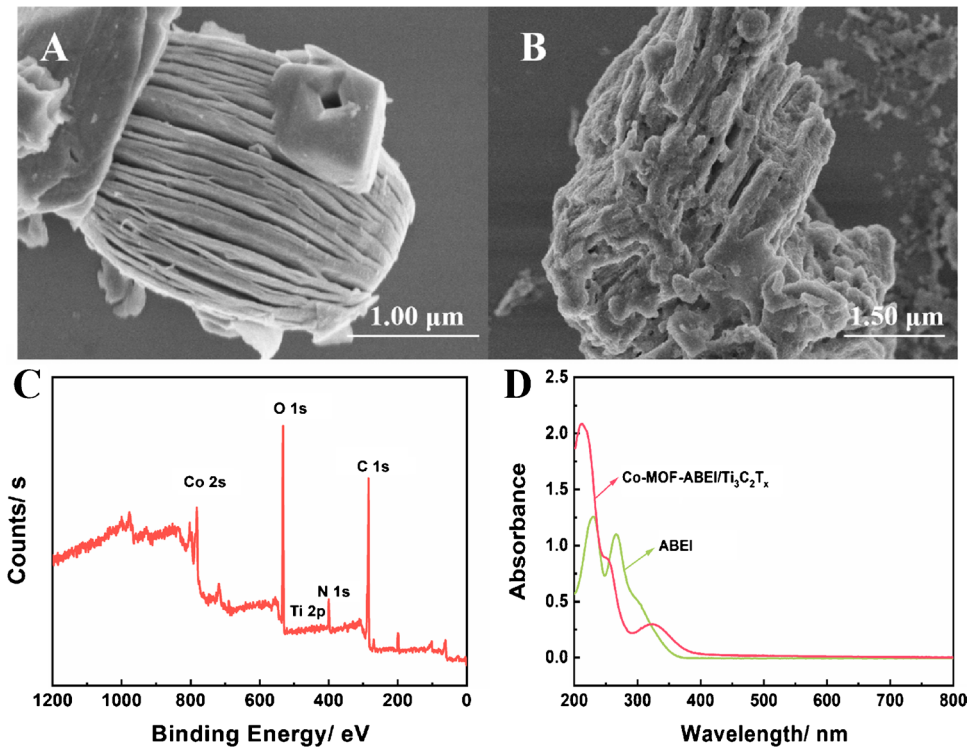

Fig. 1 SEM images of **A** $Ti_3C_2T_x$ and **B** Co-MOF-ABEI/$Ti_3C_2T_x$ composites. **C** Full XPS spectrum of the Co-MOF-ABEI/$Ti_3C_2T_x$ composite. **D** UV–vis spectra of ABEI and the Co-MOF-ABEI/$Ti_3C_2T_x$ composite

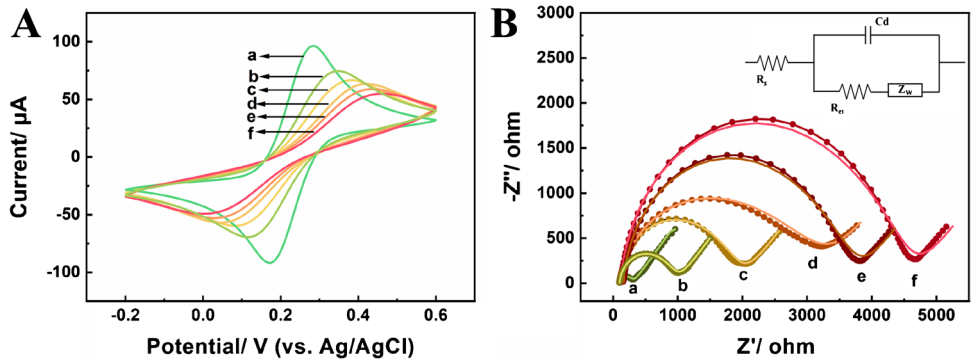

Fig. 2 **A** CV and **B** EIS results of different electrodes: (a) bare GCE, (b) Co-MOF-ABEI/$Ti_3C_2T_x$/GCE, (c) probe DNA/GA/CS/Co-MOF-ABEI/$Ti_3C_2T_x$/GCE, (d) MEA/probe DNA/GA/CS/Co-MOF-ABEI/$Ti_3C_2T_x$/GCE, (e) S2/MEA/probe DNA/GA/CS/Co-MOF-ABEI/$Ti_3C_2T_x$/GCE, and (f) hemin/S2/MEA/probe DNA/GA/CS/Co-MOF-ABEI/$Ti_3C_2T_x$/GCE. These electrochemical measurements were carried out in 0.1 M PBS (pH 7.4) containing 5.0 mM $[Fe(CN)_6]^{3-/4-}$ and 0.1 M KCl

Electrochemical characterization

To monitor and verify the fabrication of the prepared biosensor, cyclic voltammograms (CVs) and electrochemical impedance spectroscopy (EIS) experiments were performed in 0.1 M PBS (pH 7.4) containing 5.0 mM $[Fe(CN)_6]^{3-/4-}$ and 0.1 M KCl. As presented in Fig. 2A, when the CV measurement was performed with the bare GCE, a pair of well-defined reversible redox peaks were observed (curve a). After modification with Co-MOF-ABEI/$Ti_3C_2T_x$, the peak current of Co-MOF-ABEI/$Ti_3C_2T_x$/GCE exhibited a slight decrease because of the strong conductivity of TiC_2T_x in the Co-MOF-ABEI/$Ti_3C_2T_x$ composite (curve b). The redox peak current decreased after the immobilization of the probe DNA (curve c) and MEA (curve d) because both prevent electron transfer. When the S2 strands were captured by the fabricated biosensing electrode, the peak current decreased further (curve e), indicating that the S2 strands had been successfully assembled. Finally, after treatment with hemin, a hemin/G-quadruplex structure formed and was assembled on the surface of the modified GCE, resulting in a sequentially decreased peak current (curve f).

Next, EIS was employed to monitor the assembly process. As shown in Fig. 2B, the bare GCE (curve a) exhibited a markedly smaller semicircle diameter than that of Co-MOF-ABEI/$Ti_3C_2T_x$/GCE (curve b), and the diameter of the semicircle consecutively increased after the hairpin probe DNA (curve c), nonconductive MEA (curve d), and S2 strands (curve e) were sequentially incubated with the modified electrode, indicating the successful assembly of the sensing system. Finally, the semicircle diameter increased further after treatment with hemin (curve f), demonstrating that the electron transfer was hampered by the hemin/G-quadruplex because of their strong repellence to redox species. In conclusion, the CV and EIS measurements confirmed the successful fabrication of the proposed biosensor.

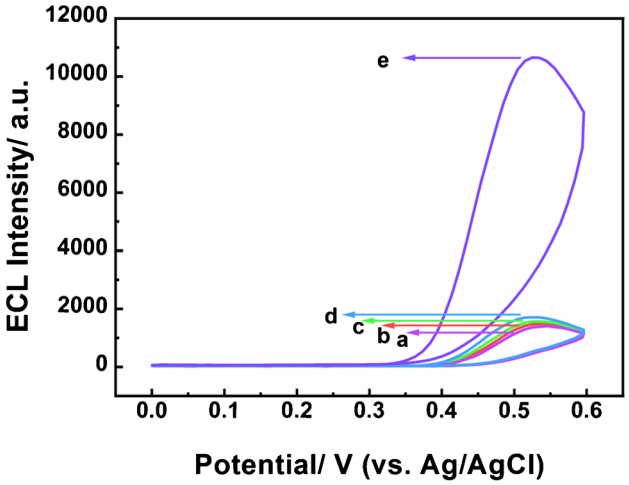

Fig. 3 ECL intensity–potential curves of probe DNA/GA/CS/Co-MOF-ABEI/$Ti_3C_2T_x$/GCE with DSN and hemin (a), with DSN and hemin but without miRNA-21 (b), with miRNA-21 and DSN but without hemin (c), with miRNA-21 and hemin but without DSN (d), and with miRNA-21, DSN, and hemin (e). The biosensor measurements were carried out in 0.1 M PBS (pH 7.4) containing 2 mM H_2O_2 by scanning from 0 to + 0.6 V at a scan rate of 0.1 $V{\cdot}s^{-1}$. The concentrations of miRNA-21, DSN, and hemin were 0.01 nM, 0.1 U, and 0.5 mM, respectively

Feasibility study

The ECL signal intensities were recorded under different conditions to verify the feasibility of the proposed ECL biosensor for real sensing applications. As shown in Fig. 3, the probe DNA/GA/CS/Co-MOF-ABEI/$Ti_3C_2T_x$/GCE exhibited low ECL signal intensity (curve a). Furthermore, in the presence of DSN and hemin but without miRNA-21, ECL signal

intensity remained almost unchanged (curve b). Without miRNA-21, the DSN cyclic amplification process cannot occur, the S2 strands cannot be released, and the probe DNA remains unopened. Consequently, no hemin/G-quadruplex is formed, and ROS are not generated. Similarly, in the presence of miRNA-21 and DSN but without hemin or in the presence of miRNA-21 and hemin but without DSN, there was no marked change in ECL signal intensity (curves c and d). This is because hemin/G-quadruplexes were still not formed. In contrast, when miRNA-21, DSN, and hemin were simultaneously present (curve e), ECL signal intensity increased significantly. These experimental results show that numerous hemin/G-quadruplex DNAzymes were formed in the presence of miRNA-21, DSN, and hemin, which promote the catalytic formation of ROS from H_2O_2 and markedly enhance ECL signal intensity. These results confirm that the proposed ECL sensing method can be used for miRNA-21 determination.

Performance optimization

To achieve optimal performance, the experimental conditions were optimized using 0.01 nM target miRNA-21; specifically, we varied the volume of the Co-MOF-ABEI/$Ti_3C_2T_x$ composite, probe DNA concentration, DSN reaction time, S1:S2 concentration, and hemin concentration. As the volume of the Co-MOF-ABEI/$Ti_3C_2T_x$ composite was increased to 10 μL, ECL signal intensity increased to the maximum. Upon further increasing the amount of the composite, ECL signal intensity changed slightly (Fig. S3A). This may be ascribed to the steric effects of the thick composite film formed. Accordingly, 10 μL was chosen as the optimal dosage. As shown in Fig. S3B, with increasing probe DNA concentration, the highest ECL signal intensity appeared at 1 μM. Thus, 1 μM of probe DNA was used for further experiments.

When the DSN reaction time was prolonged from 20 to 70 min, ECL signal intensity gradually increased and stabilized at 70 min (Fig. S3C), indicating that 70 min was sufficient for this specific reaction. Therefore, the optimal DSN reaction time was 70 min. As shown in Fig. S3D, with an increase in the concentration of the S1:S2 strands, the ECL intensity reached the maximum value at 2 μM, and this was attributed to the limited binding sites on the MBs [37]. Therefore, S1:S2 was used at a concentration of 2 μM. As the concentration of hemin increased, ECL signal intensity increased until the concentration of the former reached 0.5 mM (Fig. S3E). This suggests that the reaction of hemin with G-quadruplex had reached saturation [36]. Thus, 0.5 mM was the optimal choice of hemin in the proposed biosensor.

To confirm the excellent ECL performance of Co-MOF-ABEI/$Ti_3C_2T_x$, we also fabricated Co-MOF, ABEI/Co-MOF, and ABEI/$Ti_3C_2T_x$ composites and used them in biosensing electrodes for miRNA-21 determination (as shown in Fig. S4). All experiments were performed using 0.01 nM miRNA-21, 0.1 U DSN, and 0.5 mM hemin. Owing to the lack of luminescent substances, markedly low ECL signal intensity was achieved using the Co-MOF-based sensing system. In contrast, the ABEI/Co-MOF-based sensing system containing the ABEI luminophore conjugated with NH_2-BDC, which acts as an organic ligand for the Co-MOF, exhibited high ECL signal intensity, which can be attributed to the large surface area and possible catalysis via Co-MOFs [33]. Despite the large surface area and high electrical conductivity of $Ti_3C_2T_x$, the ABEI/$Ti_3C_2T_x$-based sensing systems yielded lower ECL signal intensity than ABEI/Co-MOF. This may be ascribed to the fact that the combination of ABEI and $Ti_3C_2T_x$ was weak, and only a small amount of ABEI was adsorbed on the surface of $Ti_3C_2T_x$ or embedded in the internal structure. For the Co-MOF-ABEI/$Ti_3C_2T_x$ sensing system, which combines the advantages of Co-MOF-ABEI and $Ti_3C_2T_x$, the highest ECL signal intensity for miRNA-21 detection was achieved, thus demonstrating the suitability of the Co-MOF-ABEI/$Ti_3C_2T_x$ composite for use in biosensing electrodes.

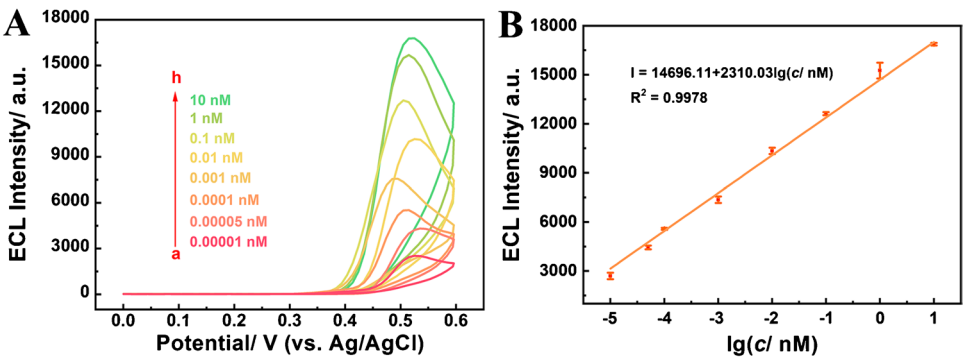

Fig. 4 **A** ECL intensity–potential curves for various concentrations of miRNA-21 (a–h, 0.00001, 0.00005, 0.0001, 0.001, 0.01, 0.1, 1, and 10 nM, respectively) and **B** calibration curve between ECL intensities and logarithm of target miRNA-21 concentrations

Detection performance

Under optimal experimental conditions, different concentrations of miRNA-21 were detected using the prepared ECL sensing platform. In Fig. 4A, it can be observed that ECL signal intensity increases with an increase in the concentration of miRNA-21 from 0.00001 to 10 nM. The obtained linear regression equation was $I = 14696.11 + 2310.03\lg(c/\text{nM})$ with a correlation coefficient of $R^2 = 0.9978$ (Fig. 4B), where I represents the ECL response and c represents the concentration of miRNA-21. The detection limit was calculated to be 3.7 fM based on the $3\sigma/a$ criterion (where a is the slope of the linear regression curve, and σ is the standard deviation of the blank analysis). In addition, a comparison of this sensing platform with other sensing methods is presented in Table S2. Combining the luminescent Co-MOF-ABEI/$Ti_3C_2T_x$ composite with the DSN-assisted signal amplification strategy resulted in both the linear detection range and limit of detection of this ECL platform being superior to those of other methods.

To test the suitability of the proposed biosensor for practical applications, its selectivity and reproducibility were evaluated. As depicted in Fig. 5A and 5B, the ECL signal intensity of miRNA-199a, miRNA-141, and miRNA-155 showed no substantial increase compared with that of the blank sample. By contrast, when a mixed solution of 0.01 nM miRNA-21 containing 0.1 nM miRNA-199a, 0.1 nM miRNA-141, and 0.1 nM miRNA-155 was used, ECL signal intensity of the biosensor was similar to that observed after incubating the biosensor with miRNA-21 (0.01 nM) alone, indicating that the interference factors had a negligible influence on the sensor response to miRNA-21. Expectedly, these results indicate that the proposed ECL biosensor exhibited outstanding selectivity.

Reproducibility is another crucial factor. Thus, nine different electrodes from the same fabrication batch were used for miRNA-21 detection. As shown in Fig. 5C, the relative standard deviation (RSD) of the detection results was less than 5.0%. Therefore, the reproducibility of the ECL biosensing method is satisfactory.

Recovery experiments and detection in real samples

To validate the practical applicability of the proposed method for the quantitative detection of miRNA-21 in complex biological matrices, a standard addition experiment was performed using human serum (10%). In the tests, three different concentrations (0.00005, 0.001, and 0.1 nM) of target miRNA-21 were added to the pretreated human serum. As displayed in Table S3, the recovery rates of the three different concentrations of the spiked miRNA-21 sample fluctuated between 96.0 and 101.8% (RSD < 4%), indicating that the proposed ECL biosensor has potential applications in complex real samples. Next, miRNA-21 extracted from the lysates of HeLa cells (human cervical cancer cells) was analyzed. As shown in Fig. 6, as the number of HeLa cells increased from 10^5 to 10^6, ECL signal intensity increased,

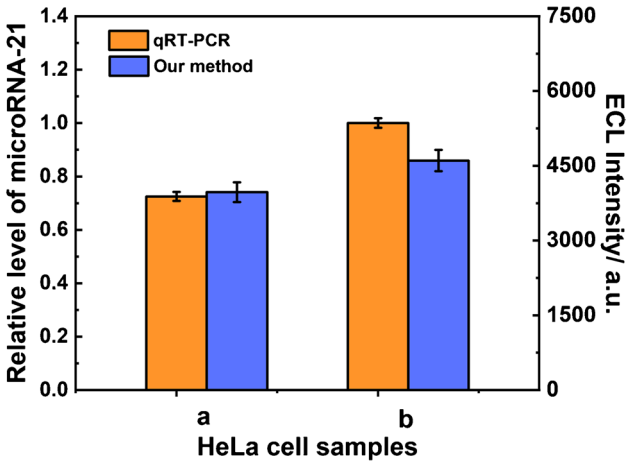

Fig. 6 Detection of miRNA-21 in total RNA extracted from HeLa cells using the presented and qRT-PCR methods: (a) 10^5 HeLa cells and (b) 10^6 HeLa cells

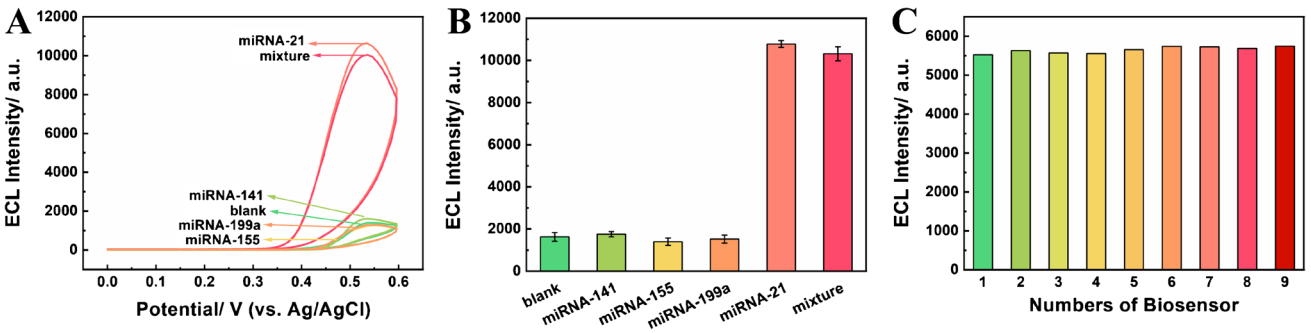

Fig. 5 **A**, **B** Specificity of the biosensor against different interfering substances: 0.1 nM of miRNA-141, miRNA-155, miRNA-199a and a mixture containing 0.1 nM of the preceding miRNAs and 0.01 nM of miRNA-21. **C** The reproducibility of nine biosensors identically fabricated for miRNA-21 (0.0001 nM)

suggesting that the cells express miRNA-21. Further measurement of the samples was performed by quantitative real-time PCR (qRT-PCR), the gold standard method for the quantitative detection of miRNA in basic and clinical research [38, 39]. The results of the qRT-PCR method and our method were consistent. Therefore, the developed biosensor has considerable potential for the clinical detection of miRNA-21.

Conclusions

An ultrasensitive ECL biosensing platform was proposed in the current study for miRNA-21 detection based on the Co-MOF-ABEI/$Ti_3C_2T_x$ composite as an ECL luminophore, a DSN cyclic amplification strategy, and the catalysis of the hemin/G-quadruplex structure. The synthesized luminescent Co-MOF-ABEI/$Ti_3C_2T_x$ carrying numerous ABEI moieties provided stable ECL signals because of the catalytic production of ROS via the hemin/G-quadruplex and increase in electrical conductivity owing to the embedded $Ti_3C_2T_x$. Combined with DSN cyclic amplification, large amounts of the hemin/G-quadruplex were formed to catalyze the conversion of H_2O_2 to ROS, which markedly amplified ECL signal intensity in the ABEI-H_2O_2 system. Expectedly, the designed ECL biosensor achieved an extremely wide dynamic detection range, high sensitivity, satisfactory selectivity, and low limit of detection for miRNA-21. Moreover, the proposed ECL method was confirmed to be accurate in 10% serum samples and was successfully applied to detect miRNA-21 extracted from HeLa cells with acceptable results, thus verifying its practical potential. Furthermore, using the design principle of this ECL biosensor, the ECL strategy can be used to develop a universal miRNA detection method by changing the structure of the S1 strand.

Supplementary Information The online version contains supplementary material available at https://doi.org/10.1007/s00604-022-05246-0.

Funding This work was supported by the National Natural Science Foundation of China (No. 22074119, 21675124, 21375102,), the National Key R&D Program of China (No. 2019YFD1002405), and the Natural Science Basic Research Program of Shaanxi (No. 2020JM-426).

Declarations

Conflict of interest The authors declare no competing interests.

References

1. Bartel DP (2018) Metazoan microRNAs. Cell 173:20–52. https://doi.org/10.1016/j.cell.2018.03.006
2. Tian H, Sun YY, Liu CH, Duan XR, Tang W, Li ZP (2016) Precise quantitation of microRNA in a single cell with droplet digital PCR based on ligation reaction. Anal Chem 88:11384–11389. https://doi.org/10.1021/acs.analchem.6b01225
3. Lu J, Getz G, Miska EA, Alvarez-Saavedra E, Lamb J, Peck D, Sweet-Cordero A, Ebert BL, Mak RH, Ferrando AA, Downing JR, Jacks T, Horvitz HR, Golub TR (2005) MicroRNA expression profiles classify human cancers. Nature 435:834–838. https://doi.org/10.1038/nature03702
4. Zampetaki A, Kiechl S, Drozdov I, Willeit P, Mayr U, Prokopi M, Mayr A, Weger S, Oberhollenzer F, Bonora E, Shah A, Willeit J, Mayr M (2010) Plasma microRNA profiling reveals loss of endothelial miR-126 and other microRNAs in type 2 diabetes. Circ Res 107:810–817. https://doi.org/10.1161/CIRCRESAHA.110.226357
5. Chen JF, Callis TE, Wang DZ (2009) microRNAs and muscle disorders. J Cell Sci 122:13–20. https://doi.org/10.1242/jcs.041723
6. Cogswell JP, Ward J, Taylor IA, Waters M, Shi Y, Cannon B, Kelnar K, Kemppainen J, Brown D, Chen C, Prinjha RK, Richardson JC, Saunders AM, Roses AD, Richards CA (2008) Identification of miRNA changes in Alzheimer's disease brain and CSF yields putative biomarkers and insights into disease pathways. J Alzheimers Dis 14:27–41. https://doi.org/10.3233/jad-2008-14103
7. Dong HF, Lei JP, Ding L, Wen YQ, Ju HX, Zhang XJ (2013) MicroRNA: function, detection, and bioanalysis. Chem Rev 113:6207–6233. https://doi.org/10.1021/cr300362f
8. Ge ZL, Lin MH, Wang P, Pei H, Yan J, Shi JY, Huang Q, He DN, Fan CH, Zuo XL (2014) Hybridization chain reaction amplification of microRNA detection with a tetrahedral DNA nanostructure-based electrochemical biosensor. Anal Chem 86:2124–2130. https://doi.org/10.1021/ac4037262
9. Bi S, Zhang JL, Hao SY, Ding CF, Zhang SS (2011) Exponential amplification for chemiluminescence resonance energy transfer detection of microRNA in real samples based on a cross-catalyst strand-displacement network. Anal Chem 83:3696–3702. https://doi.org/10.1021/ac200096b
10. Li M, Xu X, Zhou ZG, Xu GH, Xie YR, Cai QY (2020) Label-free detection of microRNA: two-stage signal enhancement with hairpin assisted cascade isothermal amplification and light-up DNA-silver nanoclusters. Microchim Acta 187:141. https://doi.org/10.1007/s00604-019-4094-1
11. Zhang YL, Li ZP, Cheng YQ, Lv XC (2009) Colorimetric detection of microRNA and RNase H activity in homogeneous solution with cationic polythiophene derivative. Chem Commun:3172-3174.https://doi.org/10.1039/b904579a
12. Xiong HT, Zheng XW (2017) Electrochemiluminescence based determination of micro-RNA using target-guided assembly of gold nanoparticles on an electrode modified with Nafion, carbon nanotubes and polyvinylpyrrolidone. Microchim Acta 184:1781–1789. https://doi.org/10.1007/s00604-017-2163-x
13. Feng QM, Shen YZ, Li MX, Zhang ZL, Zhao W, Xu JJ, Chen HY (2016) Dual-wavelength electrochemiluminescence ratiometry based on resonance energy transfer between Au nanoparticles functionalized g-C_3N_4 nanosheet and $Ru(bpy)_3^{2+}$ for microRNA detection. Anal Chem 88:937–944. https://doi.org/10.1021/acs.analchem.5b03670
14. Liu ZY, Qi WJ, Xu GB (2015) Recent advances in electrochemiluminescence. Chem Soc Rev 44:3117–3142. https://doi.org/10.1039/c5cs00086f
15. Biggar KK, Wu CW, Storey KB (2014) High-throughput amplification of mature microRNAs in uncharacterized animal models using polyadenylated RNA and stem- loop reverse transcription polymerase chain reaction. Anal Biochem 462:32–34. https://doi.org/10.1016/j.ab.2014.05.032
16. Liu HY, Li L, Duan LL, Wang X, Xie YX, Tong LL, Wang Q, Tang B (2013) High specific and ultrasensitive isothermal

detection of microRNA by padlock probe-based exponential rolling circle amplification. Anal Chem 85:7941–7947. https://doi.org/10.1021/ac401715k
17. Shuai HL, Huang KJ, Xing LL, Chen YX (2016) Ultrasensitive electrochemical sensing platform for microRNA based on tungsten oxide-graphene composites coupling with catalyzed hairpin assembly target recycling and enzyme signal amplification. Biosens Bioelectron 86:337–345. https://doi.org/10.1016/j.bios.2016.06.057
18. Xi Q, Zhou DM, Kan YY, Ge J, Wu ZK, Yu RQ, Jiang JH (2014) Highly sensitive and selective strategy for microRNA detection based on WS_2 nanosheet mediated fluorescence quenching and duplex-specific nuclease signal amplification. Anal Chem 86:1361–1365. https://doi.org/10.1021/ac403944c
19. Shuai HL, Huang KJ, Chen YX, Fang LX, Jia MP (2017) Au nanoparticles/hollow molybdenum disulfide microcubes based biosensor for microRNA-21 detection coupled with duplex-specific nuclease and enzyme signal amplification. Biosens Bioelectron 89:989–997. https://doi.org/10.1016/j.bios.2016.10.051
20. Hun X, Meng Y (2020) Electron acceptors co-regulated self-powered photoelectrochemical strategy and its application for circulating tumor nucleic acid detection coupled with recombinase polymerase amplification. Anal Chem 92(17):11771–11778. https://doi.org/10.1021/acs.analchem.0c01893
21. Cui A, Zhang J, Bai W, Sun H, Bao L, Ma F, Li Y (2019) Signal-on electrogenerated chemiluminescence biosensor for ultrasensitive detection of microRNA-21 based on isothermal strand-displacement polymerase reaction and bridge DNA-gold nanoparticles. Biosens Bioelectron 144:111664. https://doi.org/10.1016/j.bios.2019.111664
22. Oster J, Parker J, Brassard LA (2001) Polyvinyl-alcohol-based magnetic beads for rapid and efficient separation of specific or unspecific nucleic acid sequences. J Magn Magn Mater 225:145–150. https://doi.org/10.1016/S0304-8853(00)01243-9
23. Liao JY, Lu MH, Tang DP (2016) Enhanced sensitivity of quartz crystal microbalance immunosensor via back-conjugation of biofunctionalized magnetic beads with an external magnetic field. Biochem Eng J 114:279–285. https://doi.org/10.1016/j.bej.2016.07.016
24. Zhang HR, Wu MS, Xu JJ, Chen HY (2014) Signal-on dual-potential electrochemiluminescence based on luminol-gold bifunctional nanoparticles for telomerase detection. Anal Chem 86:3834–3840. https://doi.org/10.1021/ac403960g
25. Jiang X, Wang H, Wang H, Zhuo Y, Yuan R, Chai YQ (2016) Self-enhanced N- (aminobutyl)-N-(ethylisoluminol) derivative-based electrochemiluminescence immunosensor for sensitive laminin detection using PdIr cubes as a mimic peroxidase. Nanoscale 8:8017–8023. https://doi.org/10.1039/c6nr00229c
26. Jiang XY, Chai YQ, Wang HJ, Yuan R (2014) Electrochemiluminescence of luminol enhanced by the synergetic catalysis of hemin and silver nanoparticles for sensitive protein detection. Biosens Bioelectron 54:20–26. https://doi.org/10.1016/j.bios.2013.10.006
27. Ge J, Qi ZY, Zhang LL, Shen XP, Shen YM, Wang WX, Li ZH (2020) Label-free and enzyme-free detection of microRNA based on a hybridization chain reaction with hemin/G-quadruplex enzymatic catalysis-induced MoS_2 quantum dots via the inner filter effect. Nanoscale 12:808–814. https://doi.org/10.1039/c9nr08154b
28. Huang YB, Liang J, Wang XS, Cao R (2017) Multifunctional metal-organic framework catalysts: synergistic catalysis and tandem reactions. Chem Soc Rev 46:126–157. https://doi.org/10.1039/c6cs00250a
29. Yang X, Yu YQ, Peng LZ, Lei YM, Chai YQ, Yuan R, Zhuo Y (2018) Strong electrochemiluminescence from MOF accelerator enriched quantum dots for enhanced sensing of trace cTnI. Anal Chem 90:3995–4002. https://doi.org/10.1021/acs.analchem.7b05137
30. Wang SS, Zhao YY, Wang MM, Li HJ, Saqib M, Ge CH, Zhang XD, Jin YD (2019) Enhancing luminol electrochemiluminescence by combined use of cobalt-based metal organic frameworks and silver nanoparticles and its application in ultrasensitive detection of cardiac troponin I. Anal Chem 91:3048–3054. https://doi.org/10.1021/acs.analchem.8b05443
31. Bai WQ, Cui AP, Liu MZ, Qiao XZ, Li Y, Wang T (2019) Signal-off electrogenerated chemiluminescence biosensing platform based on the quenching effect between ferrocene and $Ru(bpy)_3^{2+}$-functionalized metal-organic frameworks for the detection of methylated RNA. Anal Chem 91:11840–11847. https://doi.org/10.1021/acs.analchem.9b02569
32. Sinha A, Dhanjai ZH, Huang Y, Lu X, Chen J, Jain R (2018) MXene: an emerging material for sensing and biosensing. TrAC Trends Anal Chem 105:424–435. https://doi.org/10.1016/j.trac.2018.05.021
33. Wei X, Guo J, Lian H, Sun X, Liu B (2021) Cobalt metal-organic framework modified carbon cloth/paper hybrid electrochemical button-sensor for nonenzymatic glucose diagnostics. Sensors Actuators B Chem 329:129205. https://doi.org/10.1016/j.snb.2020.129205
34. Naguib M, Kurtoglu M, Presser V, Lu J, Niu J, Heon M, Hultman L, Gogotsi Y, Barsoum MW (2011) Two-dimensional nanocrystals produced by exfoliation of Ti_3AlC_2. Adv Mater 23:4248–4253. https://doi.org/10.1002/adma.201102306
35. Yang X, Lv J, Yang ZH, Yuan R, Chai YQ (2017) A sensitive electrochemical aptasensor for thrombin detection based on electroactive Co-based metal-organic frameworks with target-triggering NESA strategy. Anal Chem 89:11636–11640. https://doi.org/10.1021/acs.analchem.7b03056
36. Liu JQ, He XX, Wang KM, He DG, Wang YH, Mao YF, Shi H, Wen L (2015) A highly sensitive electrochemiluminescence assay for protein kinase based on double- quenching of graphene quantum dots by G-quadruplex–hemin and gold nanoparticles. Biosens Bioelectron 70:54–60. https://doi.org/10.1016/j.bios.2015.03.026
37. Zhu DB, Liu JF, Tang YB, Xing D (2010) A reusable DNA biosensor for the detection of genetically modified organism using magnetic bead-based electrochemiluminescence. Sensors Actuators B Chem 149:221–225. https://doi.org/10.1016/j.snb.2010.05.047
38. Ouyang T, Liu Z, Han Z, Ge Q (2019) MicroRNA detection specificity: recent advances and future perspective. Anal Chem 91(5):3179–3186. https://doi.org/10.1021/acs.analchem.8b05909
39. Jiang X, Hao C, Zhang H, Wu X, Xu L, Sun M, Xu C, Kuang H (2021) Dual-modal Fe_xCu_ySe and upconversion nanoparticle assemblies for intracellular microRNA-21 detection. ACS Appl Mater Interfaces 13:41405–41413. https://doi.org/10.1021/acsami.0c00434